Calculus of variations/Theory of signals

Reflective filtered backprojection

CrossMark

Rétroprojection filtrée réflective

Jean-Baptiste Bellet [a], Gérard Berginc [b]

[a] *Université de Lorraine et CNRS, Institut Élie-Cartan de Lorraine, UMR 7502, 57045 Metz, France*
[b] *Thales Optronique, 2, av. Gay-Lussac, CS 90502, 78995 Élancourt cedex, France*

A R T I C L E   I N F O

A B S T R A C T

This note introduces reflective tomography in a mathematical framework. The effect of the filtered backprojection on reflective-kind projections is studied: a reflective projection is defined, tomographic filtering of such a projection is analysed, and so is the filtered backprojection. The results emphasize the role of the contrasts: we get a decomposition in which the contributions of the discontinuities and of the tangential variations are enlightened.

© 2016 Académie des sciences. Published by Elsevier Masson SAS. This is an open access article under the CC BY-NC-ND license (http://creativecommons.org/licenses/by-nc-nd/4.0/).

R É S U M É

Cette note introduit la tomographie réflective dans un cadre mathématique. Nous proposons une étude de la rétroprojection filtrée, sur des projections de type réflectif. On définit une projection réflective, le filtrage tomographique de telles données est analysé, ainsi que leur rétroprojection filtrée. Les résultats soulignent le rôle des contrastes : on obtient une décomposition dans laquelle les contributions des discontinuités et des variations tangentielles sont mises en évidence.

© 2016 Académie des sciences. Published by Elsevier Masson SAS. This is an open access article under the CC BY-NC-ND license (http://creativecommons.org/licenses/by-nc-nd/4.0/).

1. Introduction

There is a considerable interest in the development of new optical imaging systems that are able to give three-dimensional images. Potential applications range across the field of defense and security for the recognition of targets, the medical field for the detection of subcutaneous and cutaneous tumors or the field of micro-electronics for the observation of hardware components during their manufacturing. Identifying targets or objects concealed by foliage or camouflage is a critical requirement for operations in public safety, law enforcement, and defense. The most promising techniques for these tasks are 3D laser imaging techniques. In this field, 3D reconstructions are obtained through a tomographic algorithm taking into account 2D images with different angles of view [1–6]. This algorithm is derived from the filtered backprojection (FBP), which is among the most famous inversion algorithms from transmission tomography by X-rays [9]. The success of
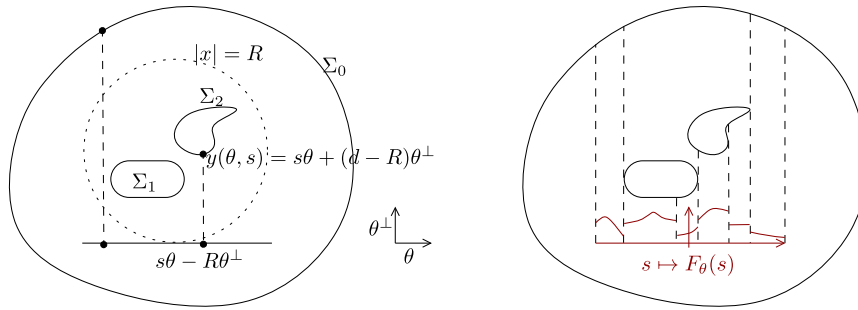
Fig. 1. Reflective projection: the opaque objects Σ_i are projected along the direction $\theta^\perp$. On the left, the dashed lines represent two rays, from a visible point $y(\theta, s)$ to the associated screen point $s\theta - R\theta^\perp$. On the right, the piecewise smooth projection $s \mapsto F_\theta(s)$ is represented.

3D laser imagery shows that FBP provides relevant results from intensity images resulting from backscattering by rough surfaces.

3D laser imagery enters in the framework of reflective tomography [8] and introduces some mathematical challenge. Indeed the standard mathematical result states that FBP inverts the Radon transform. That is the justification of transmission tomography under the complete view assumption—scan over 360 degrees. Here the previous comments suggest that FBP works also for reflective images, and does not require the complete-view assumption. This heuristically extends the domain of validity of FBP: FBP can reconstruct the boundaries of opaque objects from a partial set of projections of the scene. Nevertheless, according to the authors' knowledge, FBP on reflective data has never been studied in a mathematical framework. This is the object of this Note: we give a meaning to a reflective filtered backprojection (RFBP), we link RFBP with the objects of the scene, and we identify different kinds of contributions in RFBP.

The first part of the work is defining a notion of reflective projection, which is inspired from the applications. Some information is projected along rays from opaque objects to a screen, and for several angles of view. This information can vary with the angle; and the angle does not necessary scan a full circle. They could represent backscattered intensities, emitted by the surfaces of the scene after exterior illuminations. So we call this a *reflective projection* of an *emission intensity*, even if the model could be used for other physical problems. The main assumption that we formulate is a piecewise smooth decomposition of the projection; it is relatively weak and enables for example objects to backscatter intensities with jumps at interfaces between different materials. With this regularity assumption, it is then possible to define and to analyse standard tomographic filtering [9] on reflective projections, due to the distribution theory [7]. Filtered projections are written as functions of the variations of the intensity: its tangential derivative on the objects, and its jumps. The next step is defining and applying the filtered backprojection, which applies the adjoint of the Radon transform onto the filtered projections. We get a decomposition of the filtered backprojection in which we distinguish the contribution of the jumps and the contribution of the tangential derivative. We investigate the case of a convex object as a corollary: the contribution of the shapes is distinguished from the contribution of the tangential variations of intensity. To conclude, we provide a numerical reconstruction in which we distinguish the two types of contributions. In a word, this note shows that RFBP is some kind of sensitivity analysis: an operator that concerns variations is applied; it aims at producing high values near the objects of the scene, and especially near portions that generate coherent contrasts in the projections.

2. Reflective projection

We consider that an object is a piecewise $\mathscr{C}^1$ simple closed curve Σ in the plane. A piecewise $\mathscr{C}^1$ function $f : \Sigma \to \mathbb{R}$ is called an emission intensity of the object Σ. If σ is a counterclockwise parameterization of Σ, then on a piece where σ and $f \circ \sigma$ are smooth, the tangential derivative $\partial_\tau f$ of the emission intensity satisfies: $(f \circ \sigma)' = (\partial_\tau f) \circ \sigma \cdot |\sigma'|$. We now consider a set of n objects: Σ_i, $1 \leq i \leq n$, such that every curve Σ_i is in the exterior domain of the other curves Σ_j, $j \neq i$: see Fig. 1. Let R be such that all the curves are inside the open disk $|x| < R$. Then, we consider an object Σ_0 whose interior domain contains the open disk $|x| < R\sqrt{2}$; Σ_0 is the wall of the experiment. This convention for the wall allows one to treat the background exactly as the objects of the scene. Let $\theta \in S^1$ be a fixed angle. Every object Σ_i, $0 \leq i \leq n$, is assumed to have an emission intensity $y \in \Sigma_i \mapsto f_i(y, \theta)$. The index i denotes the number of the object, the first variable $y \in \Sigma_i$ is the emission point, whereas the second variable θ indicates that the intensity emission may depend on the angle θ. We measure on a screen the projection of the scene along lines that are orthogonal to $\theta = (\theta_1, \theta_2)$, or parallel to $\theta^\perp = (-\theta_2, \theta_1)$. For all $s \in [-R, R]$, the scene is projected on the screen, into the point $s\theta - R\theta^\perp$. The visible point is $y(\theta, s)$, which is the first intersection point of the line $L(\theta, s) = \{x \cdot \theta = s\}$ with the objects: $y(\theta, s) = \arg\min\{y \cdot \theta^\perp : y \cdot \theta^\perp - R > 0, y \in L(\theta, s) \cap \cup_{0 \leq i \leq n} \Sigma_i\}$. The measurement is the emission intensity of the point $y(\theta, s)$: $F_\theta(s) = f_{i(\theta, s)}(y(\theta, s), \theta)$, where $i(\theta, s) \in [0, n]$ denotes the object number of $y(\theta, s)$. The function $s \mapsto F_\theta(s)$ is a one-dimensional image that we call the reflective projection, associated with the angle θ. The process of reflective projection is illustrated in Fig. 1; this figure also contains an example of a one-dimensional image F_θ.

Notation 2.1. We denote by E the space of functions $g : [-R, R] \mapsto \mathbb{R}$ that are piecewise $\mathscr{C}^1$ and whose pieces can be extended by continuity: $g \in E$ if, and only if, there exists a (finite) subdivision $-R = s_0 < \cdots < s_j < \cdots < s_{N+1} = R$ and there exists a family of functions $g_j \in \mathscr{C}^1((s_j, s_{j+1})) \cap \mathscr{C}^0([s_j, s_{j+1}])$, $0 \le j \le N$, such that $\forall s \notin \{s_j, j\}$, $g(s) = \sum_{j=0}^N g_j(s) \mathbb{1}_{(s_j, s_{j+1})}(s)$. For convenience, we extend $g \in E$ by zero: $g(s) = 0$ for $|s| > R$.

We assume that the projection F_θ belongs to the space E, with the following piecewise smooth decomposition:

$$F_\theta(s) = \sum_{j=0}^{n_\theta} f_{i(\theta, j)}(y(\theta, s), \theta) \mathbb{1}_{(s(\theta, j), s(\theta, j+1))}(s), \tag{2.1}$$

with $-R = s(\theta, 0) < \cdots < s(\theta, j) < s(\theta, j+1) < \cdots < s(\theta, n_\theta + 1) = R$. On the piece $(s(\theta, j), s(\theta, j+1))$, the visible part of the scene is $\Sigma(\theta, j)$, subset of the object number $i(\theta, j)$: $\Sigma(\theta, j) := \{y(\theta, s), s \in (s(\theta, j), s(\theta, j+1))\} \subset \Sigma_{i(\theta, j)}$. The piece $\Sigma(\theta, j)$ is furthermore assumed to be $\mathscr{C}^1$. As in the Fig. 1, the following reasons explain the apparition of jumps in the projection F_θ:

- geometrical jump: the consecutive visible pieces $\Sigma(\theta, j)$ and $\Sigma(\theta, j+1)$ are not linked: $y(\theta, s)$ jumps from one object to another object, or jumps from one part of a non-convex object to another part of the same object;
- tangential jump: the pieces $\Sigma(\theta, j)$ and $\Sigma(\theta, j+1)$ are included in the same object Σ_i and are linked, and so $y(\theta, s)$ is continuous, but the emission intensity of the object f_i jumps.

Finally, we change the acquisition angle and we restart: this experiment is repeated for θ moving in a finite set of angles $\Theta \subset S^1$. Juxtaposing the different images, we get at the end a reflective sinogram $(s, \theta) \mapsto F_\theta(s)$. In the sinogram, each emission point $y \in \cup_{0 \le i \le n} \Sigma_i$ is seen partially (or eventually not seen) on the sinusoid $y \cdot \theta = s$; its intensity level depends on θ.

3. From tomographic filtering to reflective filtered backprojection

Definition 3.1. A regularized kernel of the Hilbert transform is $\phi = \mathcal{F}^{-1}(-\mathrm{i}\,\mathrm{sign}(\sigma) \cdot \hat{h}(\sigma))$, where $\mathcal{F}$ is the Fourier transform and $\hat{h}(\sigma)$ is an even windowing function with compact support (σ is the frequency).

Proposition 3.1. *Such a kernel ϕ is odd and belongs to $\mathscr{C}^\infty$ (with low-growing derivatives).*

Definition 3.2 (*Tomographic filtering*). Let $f \in E$ (extended by zero). Since f is in the space $\mathcal{E}'$ of distributions with compact support, it makes sense to define the tomographic ϕ-filtering $\partial_s f \star \phi$ of f, and:

$$\partial_s f \star \phi = \mathcal{F}^{-1}(|\sigma| \hat{h}(\sigma) \mathcal{F}(f)(\sigma)).$$

Lemma 3.3. *Let $f \in E$, with the following decomposition in E: $f(s) = \sum_{j=0}^N f(s) \mathbb{1}_{(s_j, s_{j+1})}(s)$. The tomographic ϕ-filtering of f is $\mathscr{C}^\infty$ and satisfies:*

$$\partial_s f \star \phi(s) = \sum_{j=0}^N \int_{s_j}^{s_{j+1}} \partial_s f(t) \phi(s - t) \mathrm{d}t + \sum_{j=0}^{N+1} [f]_j \phi(s - s_j),$$

where $[f]_j := f(s_j+) - f(s_j-)$ is the jump of f across s_j.

Proof. This result is a consequence of the jumps formula in the sense of distributions. It states that: $\partial_s f = \sum_{j=0}^N \partial_s f(s) \mathbb{1}_{(s_j, s_{j+1})}(s) + \sum_{j=0}^{N+1} [f]_j \delta_{s_j}$. As $\partial_s f \in \mathcal{E}'$, it can be convolved with $\phi \in \mathscr{C}^\infty$. We get the following $\mathscr{C}^\infty$ function:

$$\partial_s f \star \phi(s) = \langle \partial_s f(t), \phi(s - t) \rangle = \sum_{j=0}^N \int_{s_j}^{s_{j+1}} \partial_s f(t) \phi(s - t) \mathrm{d}t + \sum_{j=0}^{N+1} [f]_j \phi(s - s_j). \quad \square$$

Theorem 3.4 (*Reflective tomographic filtering*). *The tomographic ϕ-filtering of the reflective projection $F_\theta \in E$ satisfies:*

$$\partial_s F_\theta \star \phi(s) = \sum_{j=0}^{n_\theta} \int_{\Sigma(\theta, j)} \partial_\tau f_{i(\theta, j)}(y, \theta) \phi(s - y \cdot \theta) \mathrm{d}\sigma(y) + \sum_{j=0}^{n_\theta + 1} [f_{\theta, j}] \phi(s - s(\theta, j)),$$

where $\partial_\tau f_{i(\theta, j)}$ is the tangential derivative of the emission intensity on the visible piece $\Sigma(\theta, j)$ and $[f_{\theta, j}]$ is an intensity jump between two pieces.

Proof. By assumption, the projection $F_\theta \in E$ has the decomposition (2.1). We apply Lemma 3.3:

$$\partial_s F_\theta = \sum_{j=0}^{n_\theta} \partial_s f_{i(\theta,j)}(y(\theta,s),\theta)\mathbb{1}_{(s(\theta,j),s(\theta,j+1))} + \sum_{j=0}^{n_\theta+1} [f_{\theta,j}]\delta_{s(\theta,j)}, \text{ with}$$

$$\partial_s f_{i(\theta,j)}(y(\theta,s),\theta) = \partial_\tau f_{i(\theta,j)}(y(\theta,s),\theta)\,|\partial_s y(\theta,s)|,$$

$$[f_{\theta,j}] := f_{i(\theta,j)}(y(\theta,s(\theta,j)+),\theta) - f_{i(\theta,j-1)}(y(\theta,s(\theta,j)-),\theta), \quad 1 \le j \le n_\theta,$$

$$[f_{\theta,0}] := f_{i(\theta,0)}(y(\theta,s(\theta,0)+),\theta), \quad [f_{\theta,n_\theta+1}] := -f_{i(\theta,n_\theta)}(y(\theta,s(\theta,n_\theta+1)-),\theta).$$

Thus the filtering is:

$$\partial_s F_\theta \star \phi(s) = \sum_{j=0}^{n_\theta} \int_{s(\theta,j)}^{s(\theta,j+1)} \partial_\tau f_{i(\theta,j)}(y(\theta,t),\theta)\,|\partial_s y(\theta,t)|\,\phi(s-t)\mathrm{d}t + \sum_{j=0}^{n_\theta+1} [f_{\theta,j}]\phi(s-s(\theta,j))$$

$$= \sum_{j=0}^{n_\theta} \int_{\Sigma(\theta,j)} \partial_\tau f_{i(\theta,j)}(y,\theta)\phi(s-y\cdot\theta)\mathrm{d}\sigma(y) + \sum_{j=0}^{n_\theta+1} [f_{\theta,j}]\phi(s-s(\theta,j)) \quad (y(\theta,t)\cdot\theta = t). \qquad \square$$

This theorem shows that a filtered image $\partial_s F_\theta \star \phi$ contains two contributions. The first one is a ϕ-spreading of the tangential variations $\partial_\tau f_{i(\theta,j)}$ of the emission intensity of the visible pieces $\Sigma(\theta,j)$. The other one is a ϕ-spreading of the intensity jumps $[f_{\theta,j}]$ between pieces. In particular, it can be noticed that when the support of ϕ is small, the last contribution is a contour detection (zero-crossing) in the image F_θ. The next step is the backprojection, which is a summation over sinusoids $x\cdot\theta = s$ in the filtered sinogram:

Definition 3.5 *(Filtered backprojection).* Let ϕ be a regularized Hilbert kernel and a sinogram $F : \theta \in \Theta \mapsto F_\theta \in E$. The filtered backprojection of F is:

$$x \in \mathbb{R}^2 \mapsto \mathcal{R}^*[\partial_s F_\theta \star \phi](x) = \sum_{\theta\in\Theta} \partial_s F_\theta \star \phi(x\cdot\theta).$$

Using the decomposition of the reflective tomographic filtering (Theorem 3.4), we get the following decomposition in the reflective case.

Theorem 3.6 *(Reflective filtered backprojection).* *If $F : \theta \in \Theta \mapsto F_\theta$ is the reflective sinogram (2.1), then its filtered backprojection with the kernel ϕ is:*

$$\mathcal{R}^*[\partial_s F_\theta \star \phi](x) = \sum_{\theta\in\Theta}\left[\sum_{j=0}^{n_\theta}\int_{\Sigma(\theta,j)} \partial_\tau f_{i(\theta,j)}(y,\theta)\phi((x-y)\cdot\theta)\mathrm{d}\sigma(y) + \sum_{j=0}^{n_\theta+1} [f_{\theta,j}]\phi(x\cdot\theta - s(\theta,j))\right].$$

This theorem shows that the reflective filtered backprojection (RFBP) contains two contributions. The first one is due to the tangential variations of the visible emission intensity, and the second one is due to the jumps. Furthermore the RFBP is a superposition of plane waves: $x \mapsto A(y,\theta)\phi((x-y)\cdot\theta)$, with $(\theta,y) \in \Theta \times \cup_i \Sigma_i$. At a *generical* point x, the contributions from different (θ,y) are generically incoherent and may compensate for each other. But coherence can appear for specific choices of x; more particularly, when the receptor x is close to a *source* y, the different (y,θ) can produce terms that are constructively added. This suggests that the highest (absolute) values of the RFBP must be located near the objects, and more particularly near points at the origin of variations or jumps in the reflective projections. Quantifying precisely the processes of accumulation and compensation of the plane waves decomposition could be subject to further studies.

Corollary 3.7 *(Convex Lambertian object).* *We consider a scene with a unique convex object Σ. We assume that its intensity $f : y \in \Sigma \mapsto f(y)$ does not depend on θ (Lambertian object). We assume that the wall Σ_0 does not emit: $f_0 = 0$. For each angle of projection $\theta \in \Theta$, the reflective projection F_θ can be decomposed in E under the form:*

$$F_\theta(s) = \sum_{j=1}^{n_\theta-1} f(y(\theta,s))\mathbb{1}_{(s(\theta,j),s(\theta,j+1))}(s),$$

with $\Sigma_+(\theta) = \{y \in \Sigma : \tau_y \cdot \theta > 0\} = \{y(\theta,s), s_1 < s < s_{n_\theta}\} = (\underline{y}_\theta, \overline{y}_\theta)$ being the visible part of Σ under the angle θ, and $\underline{y}_\theta, \overline{y}_\theta \in \Sigma$ being the boundary points of $\Sigma_+(\theta)$. We also introduce the finite set of boundary points where f jumps: $y_\alpha, \alpha \in A$, and the jumps: $[f_\alpha]$. The decomposition of the RFBP yields: $\mathcal{R}^*[\partial_s F_\theta \star \phi](x) = T_{\text{der}} + T_{\text{jump}} + S_{\text{left}} + S_{\text{right}}$, with:
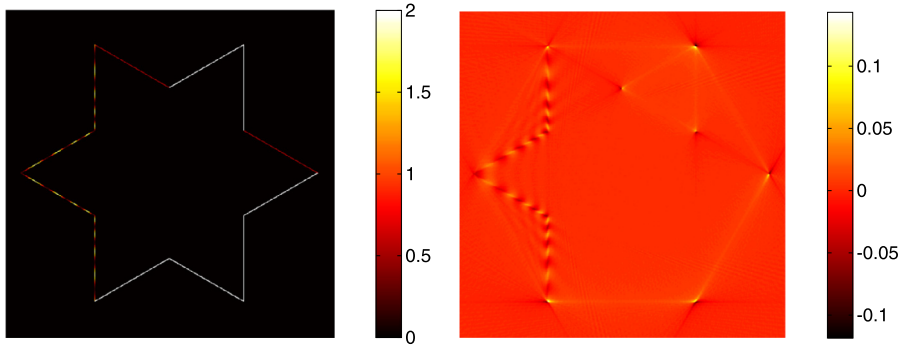
Fig. 2. The object f is on the left and FBP of the resulting reflective sinogram is on the right.

$$T_{\mathrm{der}} = \int_{\Sigma} \partial_\tau f(y) \sum_{\theta \in \Theta : \theta \cdot \tau > 0} \phi((x - y) \cdot \theta) \mathrm{d}\sigma(y); \qquad T_{\mathrm{jump}} = \sum_{\alpha \in A} [f_\alpha] \sum_{\substack{\theta \in \Theta : \theta \cdot \tau_{y_\alpha} > 0, \\ s(\theta,1) < y_\alpha \cdot \theta < s(\theta, n_\theta)}} \phi((x - y_\alpha) \cdot \theta);$$

$$S_{\mathrm{left}} = \sum_{\theta \in \Theta} f(\underline{y}_\theta) \phi((x - \underline{y}_\theta) \cdot \theta); \qquad S_{\mathrm{right}} = \sum_{\theta \in \Theta} -f(\overline{y}_\theta) \phi((x - \overline{y}_\theta) \cdot \theta).$$

The term T_{der} looks like a convolution of the tangential derivative of the intensity f with a partial backprojection of the filter ϕ; for each *source* $y \in \Sigma$, only the angles θ such that y is visible under θ are kept in the backprojection. The term T_{jump} is very similar but is about the tangential jumps $[f_\alpha]$ at the points $y_\alpha \in \Sigma$. The term S_{left}, resp. S_{right}, comes from the jumps at the left, resp. right, boundaries $s(\theta, 1)$, resp. $s(\theta, n_\theta)$, of the object in the images F_θ. As a result, the RFBP has two contributions: $S_{\mathrm{left}} + S_{\mathrm{right}}$ which is mainly due to the shapes of Σ, and $T_{\mathrm{der}} + T_{\mathrm{jump}}$ which is due to the tangential variations (and jumps) of the intensity f.

4. Example

We consider a star whose intensity f does not depend on θ (Fig. 2). The scene is projected every degree: $\Theta \equiv \{i \frac{2\pi}{360}, 0 \leq i \leq 359\}$, inside a black wall: $f_0 = 0$. We observe that the support of the reconstruction is well located, up to some arte-facts. We observe the two contributions of RFBP. The vertices introduce jumps, in particular at the interface star–background and at interfaces between adjacent edges (top right). That is why the reconstruction has peaks located at vertices. Also the smooth variations (left) produce a contrasted reconstruction, despite the concavities. Obviously, we also observe that a binary non-convex part is not recovered (bottom right). The key of the method is indeed jumps and variations.

References

[1] J.-B. Bellet, I. Berechet, S. Berechet, G. Berginc, G. Rigaud, Laser interactive 3D computer graphics, in: Proc. 2nd International Conference on Tomography of Materials and Structures, Québec, Canada, 2015, https://hal.archives-ouvertes.fr/hal-01175855.
[2] G. Berginc, Scattering models for range profiling and 2D–3D laser imagery, in: L.M. Hanssen (Ed.), Reflection, Scattering, and Diffraction from Surfaces IV, 92050K, Proc. SPIE 9205 (2014).
[3] G. Berginc, M. Jouffroy, Optronic system and method dedicated to identification for formulating three-dimensional images, November 2009, US patent No. 20110254924 A1, European patent No. 2333481 A1, FR 09 05720 B1.
[4] G. Berginc, M. Jouffroy, Simulation of 3D laser systems, in: Geoscience and Remote Sensing Symposium, 2009 IEEE International, IGARSS 2009, vol. 2, IEEE, 2009, pp. 440–444.
[5] G. Berginc, M. Jouffroy, Simulation of 3D laser imaging, PIERS Online 6 (5) (2010) 415–419.
[6] G. Berginc, M. Jouffroy, 3D laser imaging, PIERS Online 7 (5) (2011) 411–415.
[7] J.-M. Bony, Cours d'analyse : théorie des distributions et analyse de Fourier, Les Éditions de l'École polytechnique, Paris, 2001.
[8] F. Knight, S. Kulkarni, R. Marino, J. Parker, Tomographic techniques applied to laser radar reflective measurements, Linc. Lab. J. 2 (2) (1989) 143–160.
[9] F. Natterer, F. Wübbeling, Mathematical Methods in Image Reconstruction, SIAM, 2001.